**Eur**opean **J**ournal of **Chem**istry

APH ATLANTA PUBLISHING HOUSE

# Synthesis, crystal structure elucidation, Hirshfeld surface analysis, 3D energy frameworks and DFT studies of 2-(4-fluorophenoxy) acetic acid

Akhileshwari Prabhuswamy [1], Yasser Hussein Eissa Mohammed [2], Fares Hezam Al-Ostoot [2,3], Geetha Doddanahalli Venkatesh [1], Sridhar Mandayam Anandalwar [1,*], Shaukath Ara Khanum [2] and Lokanath Neratur Krishnappagowda [1]

[1] Department of Studies in Physics, Manasagangotri, University of Mysore, Mysuru 570 006, India
akhila@uomphysics.net (A.P.), geetha@uomphysics.net (G.D.V.), mas@physics.uni-mysore.ac.in (S.M.A.), lokanath@physics.uni-mysore.ac.in (L.N.K.)
[2] Department of Chemistry, Yuvaraja's College, University of Mysore, Mysuru 570 006, India
issayasser16@gmail.com (Y.H.E.M.), faresalostoot@gmail.com (F.H.A.), shaukathara@yahoo.co.in (S.A.K.)
[3] Department of Biochemistry, Faculty of Education and Science, Al-Baydha University, Yemen

* Corresponding author at: Department of Studies in Physics, Manasagangotri, University of Mysore, Mysuru 570 006, India.
 e-mail: mas@physics.uni-mysore.ac.in (S.M. Anandalwar).

**RESEARCH ARTICLE**

**ABSTRACT**

The compound 2-(4-fluorophenoxy) acetic acid was synthesized by refluxing, 4-fluoro-phenol as a starting material with ethyl chloroacetate in acetone as solvent. The compound crystallizes in the monoclinic crystal system with the space group $P2_1/c$. Crystal data for $C_8H_7FO_3$, a = 13.3087(17) Å, b = 4.9912(6) Å, c = 11.6018(15) Å, β = 104.171(4)°, V = 747.21(16) Å³, Z = 4, T = 293(2) K, μ(CuKα) = 1.142 mm$^{-1}$, Dcalc = 1.512 g/cm³, 8759 reflections measured (13.72° ≤ 2Θ ≤ 130.62°), 1246 unique ($R_{int}$ = 0.0528) which were used in all calculations. The final R1 was 0.0458 (>2sigma(I)) and wR2 was 0.1313 (all data). The structure was stabilized by C-H···O and C-H···Cg interactions. The intermolecular interactions in the crystal were studied using Hirshfeld surface analysis. 3D energy frameworks were computed to visualize the packing modes. DFT calculations were performed. The FMOs were studied to estimate the kinetic stability and reactivity of the molecule. The MEP surface was generated to investigate the charge distribution and chemical reactive sites in the molecule.

**KEYWORDS**

**Cite this**: *Eur. J. Chem.* **2021**, *12(3)*, 304-313 | **Journal website**: www.eurjchem.com

## 1. Introduction

Organic synthesis is one of the most important sources of new compounds that have the ability to bind and shape new items with new chemical and physical properties that affect our daily life in medicine, agriculture, and life in general [1-3]. Phenoxy acids are unquestionably among the most significant functional groups in organic chemistry. They are present, among several other structures, in certain naturally occurring particles, synthesized polymers, peptides, and pharmaceutical agents [4-7]. The formation of phenoxy acid bonds was one of the most significant pharmaceutical synthesis transformations [8,9], taking into account a high percentage of all preliminary evaluation responses in industrial and medical applications laboratories as recently reported [10]. The true usefulness of phenoxy systems for medicinal chemists is the ability to synthesize one library based on a particular core scaffold and screen it against a wide range of different receptors, gaining several active compounds. Phenoxy acid analogs are considered really significant substances in medicinal chemistry. The molecules have also been found to provide a great antifungal event against microorganisms. They also have moderate activity against Gram-negative bacteria compared to regular standard ciprofloxacin [11]. Compounds with a phenoxy acetamide core structure have attracted considerable interest as these derivatives have established a wonderful range of pharmacological potentials such as anti-inflammatory, anti-bacterial, anti-parasitic, anti-cancer, anti-viral and anti-hypoglycemic effects [12-20]. The effects of aryloxyaliphatic acid on blood vessel permeability and the antimicrobial action of phenoxyacetic acid against human pathogens have been recorded. Azomethine and its phenoxy acetic acid-derived complexes have reported biological importance including pyridoxal phosphate anti-metabolites, bacteriostatic activity, and antitumor activity [21-26]. In view of their broad spectrum of medicinal properties and as a part of our ongoing work on the synthesis and characterization of novel compounds [27-29], the title compound was synthesized.
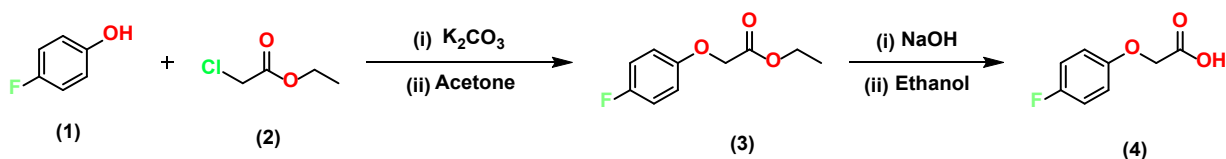
**Figure 1.** Schematic representation of the synthesis of the title compound.
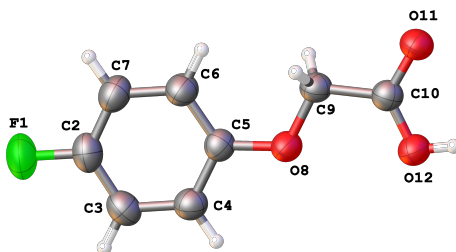


**Figure 2.** ORTEP diagram of the molecule drawn at 50% probability.

The compound obtained was characterized spectroscopically, and the structure was confirmed by X-ray diffraction studies. The crystal structure characterization of the title compound was previously reported by Smith *et al.* [30]. Hirshfeld surface analysis and DFT study of the title compound were presented in this article.

## 2. Experimental

### 2.1. Instrumentation

The chemicals required for the synthesis of the title compound were procured from M/S Sigma-Aldrich Chemical Co. The reaction progress was checked by thin layer chromatography (TLC) which was performed on aluminum-backed silica plates and the spots were detected by exposure to UV-light at $\lambda$ = 254 nm. The melting point and the boiling point were measured in a Chemiline Microcontroller-Based Melting Point/Boiling Point-CL725 apparatus with a digital thermometer. The IR spectrum was recorded on the Agilent Technologies Cary 630 FTIR spectrometer, $^1H$ and $^{13}C$ NMR spectra were recorded on a VNMRS-400 Agilent-NMR spectrophotometer. The mass spectrum was obtained with a VG70-70H spectrometer and elemental analysis (C, H, and N) was performed on an elemental analyzer Elementar Vario EL III. The results of the elemental analysis are within ±0.5% of the theoretical values.

### 2.2. Synthetic procedure for 2-(4-fluorophenoxy) acetic acid

The compound 2-(4-fluorophenoxy) acetic acid was synthesized by refluxing 4-fluorophenol as a starting material with ethyl chloroacetate in acetone as solvent to achieve the corresponding ester as 4-fluorophenoxy ethyl acetate (**3**). This was followed by hydrolysis with sodium hydroxide in the presence of ethanol.

A mixture of 4-fluorophenol (0.04 mol), ethyl chloroacetate (0.040 mol) and anhydrous potassium carbonate (0.04 mol) in dry acetone (50 mL) was refluxed for 10 hours. Then the reaction mixture was cooled and the solvent was removed by distillation. The residual mass was triturated with cold water to remove potassium carbonate and extracted with ether (3×30 mL). The organic layer was then washed with 10% sodium hydroxide solution (3×30 mL) followed by water (3×30 mL) and dried over anhydrous sodium sulphate and evaporated to give the corresponding 4-fluoro phenoxy ethyl acetate ester (**3**).

The compound **3** (0.015 mol) was then dissolved in ethanol (15 mL) with sodium hydroxide as solvent (0.030 mol), then

water (5 mL) was added to the reaction mixture. The reaction was monitored by TLC using a hexane: ethyl acetate: methanol (5:2:1) system. The mixture was refluxed for 8 hours and the reaction mixture was cooled and acidified with 2 N hydrochloric acid [31,32]. The precipitate was filtered off and washed with water, and finally recrystallized from ethanol to yield a colorless needle-like crystal. The schematic representation of the synthesis of the title compound is shown in Figure 1.

2-(4-Fluorophenoxy) acetic acid: Yield: 75%. M.p.: 105-107 °C. FT-IR (KBr, $\nu$, cm$^{-1}$): 1730-1760 (C=O), 1245-1255 (Ar-O-C), 3350-3375 (OH). $^1H$ NMR (400 MHz, DMSO-$d_6$, $\delta$, ppm): 4.67 (s, 2H, OCH$_2$), 6.55-7.55 (d, 4H, Ar-H), 13.03 (bs, 1H, OH). LC-MS (*m/z*): 171 [M+1]. Anal. calcd. for $C_8H_7FO_3$: C, 56.46; H, 4.14. Found: C, 56.38; H, 4.08%.

### 2.3. X-ray diffraction analysis

Single crystal X-ray diffraction study was carried out to determine the unit cell parameters. A colorless single crystal of the title compound with appropriate dimension 0.22×0.21× 0.20 mm was used to study the X-ray diffraction. XRD analysis reveals that the title compound $C_6H_7O_3F$ crystallizes in the monoclinic crystal system with the space group $P2_1/c$. The reflections were collected on a Rigaku XtaLAB mini diffractometer equipped with CuKα radiation with the wavelength 1.54178 Å. The data reductions of all measured reflections were carried out using the *CrystalClear* software [33]. Crystal structure was solved by direct method using SHELXS-97 and refined by full-matrix least squares on $F^2$ using SHELXL-97 [34]. The positions of the hydrogen atoms attached to the carbon atoms were generated geometrically. Hydrogen atoms are allowed to ride on their parent atoms. All non-H atoms were refined anisotropically. A total of 110 parameters were refined with 1246 unique reflections. The residual factor R converged to 0.0458 and the wR2 was 0.1313 for all data. Geometrical calculations were performed using PLATON [35]. The ORTEP of the molecule with thermal ellipsoids drawn at 50% probability is shown in Figure 2. The molecular and packing diagrams were generated using MERCURY [36]. The crystal data was deposited at the Cambridge Crystallographic Data Center (CCDC) as deposition number 1949545.

## 3. Results and discussions

### 3.1. Crystal structure description

The title compound crystallizes in the monoclinic crystal system with the space group $P2_1/c$.
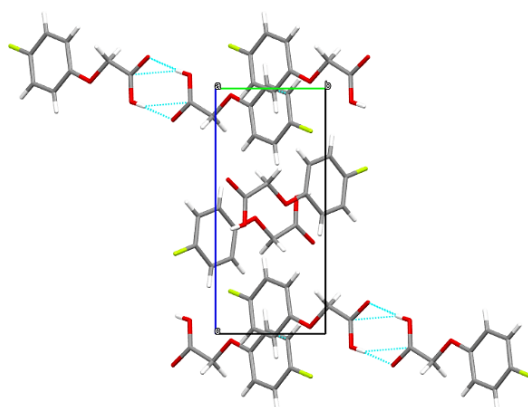
**Table 1**. Crystal data and structure refinement details.

| | |
|---|---|
| CCDC Number | 1949545 |
| Empirical formula | $C_8H_7FO_3$ |
| Formula weight | 170.14 |
| Temperature (K) | 293(2) |
| Crystal system | Monoclinic |
| Space group | $P2_1/c$ |
| a (Å) | 13.3087(17) |
| b (Å) | 4.9912(6) |
| c (Å) | 11.6018(15) |
| β (°) | 104.171(4) |
| Volume (Å³) | 747.21(16) |
| Z | 4 |
| $\rho_{calc}$ (g/cm³) | 1.512 |
| μ (mm⁻¹) | 1.142 |
| F(000) | 352.0 |
| Crystal size (mm³) | 0.22 × 0.21 × 0.20 |
| Radiation | CuKα (λ = 1.54178) |
| 2θ range for data collection (°) | 13.72 to 130.62 |
| Index ranges | -15 ≤ $h$ ≤ 15, -5 ≤ $k$ ≤ 5, -13 ≤ $l$ ≤ 13 |
| Reflections collected | 8759 |
| Independent reflections | 1246 [$R_{int}$ = 0.0528] |
| Data/restraints/parameters | 1246/0/110 |
| Goodness-of-fit on F² | 1.108 |
| Final R indexes [I≥2σ (I)] | $R_1$ = 0.0458, w$R_2$ = 0.1295 |
| Final R indexes [all data] | $R_1$ = 0.0472, w$R_2$ = 0.1313 |
| Largest diff. peak/hole (e Å⁻³) | 0.30/-0.27 |

**Table 2.** Geometry of hydrogen bond interactions.

| D-H...A | D-H (Å) | H⋯A (Å) | D⋯A (Å) | D-H⋯A (°) |
|---|---|---|---|---|
| C12-H12⋯O11ⁱ | 0.82 | 1.82 | 2.636(1) | 172 |
| C9-H9B⋯O11ⁱⁱ | 0.97 | 2.42 | 3.249(2) | 144 |

Symmetry codes: i = 2-*x*, -1-*y*, -*z*; ii =2-*x*, 1/2+*y*, 1/2-*z*.



**Figure 3.** Packing of molecules viewed along the *b* axis.

The unit cell parameters are *a* = 13.3087(17) Å, *b* = 4.9912(6) Å, *c* =11.6018(15) Å, and β = 104.171(4)°. Crystal data and structure refinement details are listed in Table 1. The values of bond length, bond angle, and torsion angles obtained by the X-ray diffraction studies are given in the CIF file.

The structure consists of a hexagonal ring (C2-C3-C4-C5-C6-C7) that is planar with a maximum deviation of 0.007(2) Å for C3 atom from the mean plane. The six-membered ring (C2-C3-C4-C5-C6-C7) is *sp²* hybridized. The crystal structure exhibits intermolecular hydrogen bonds of the type O-H⋯O and C-H⋯O whose symmetry codes are 2-*x*, -1-*y*, -*z* and 2-*x*, 1/2+*y*, 1/2-*z*, respectively.

In the structure, the C5-O8 bond length is 1.379(2) Å, which signifies a typical single bond, whereas the C10-O11 bond length is 1.261(2) Å indicates the double bond. The torsion angles for C9-O8-C5-C4 (-176.1(1)°) and C9-O8-C5-C6 (4.8(2)°) indicate the *anti*-periplanar and *syn*-clinal conformations, respectively.

The molecular structure exhibits a short ring Cg⋯Cg interaction. cg is the centroid of the ring C2-C3-C4-C5-C6-C7 with Cg⋯Cg distance of 4.7992(1) Å, and perpendicular distance of cg on itself is -3.1529(1) Å with a slippage value of

3.623 Å. The symmetry code for the Cg⋯Cg interaction is 1-*x*, 1-*y*, -*z*. The structure further involves C-F...cg interaction; C2-F1 atoms and the centroid of the ring (C2-C3-C4-C5-C6-C7). The F1-cg distance is 3.7787(2), and γ is 21.47°, C2-cg distance is 4.214(2) Å, and C2-F⋯Cg angle is 99.05(1)° with the symmetry code *x*, 1+*y*, *z*.

The structure is stabilized by C-H...cg interactions. The distance between H-Cg (H9A⋯Cg) is 2.67 Å, γ = 8.68°, and C9-Cg distance is 3.4245(2) Å. The angle of deviation of C9-H9A from the π plane is 134°.

The molecules are further connected by C-H⋯O and O-H⋯O intermolecular interactions. Hydrogen bond interactions are listed in Table 2. The packing of the molecules when viewed along the *b* axis is shown in Figure 3.

### 3.2. Hirshfeld surface analysis

The Hirshfeld surface analysis is the visualization of intermolecular interactions between the molecules in a crystal. It helps to anatomize the interplanar distance, angles, and packing modes in the crystal.
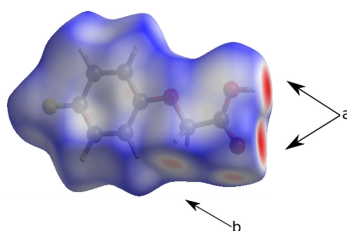
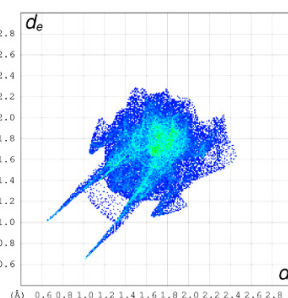**Figure 4.** Hirshfeld surface of the molecule mapped over $d_{norm}$.



**Figure 5.** 2D fingerprint plot of all intermolecular contacts.

The Hirshfeld surface of a molecule divides the electron density of a crystal into molecular fragments. It divides the crystal into regions where the electron distribution of a sum of spherical atoms for the molecule (the promolecule) dominates the corresponding sum over the crystal (the procrystal) [37]. The Hirshfeld surface is generated for the molecule and the proximity of its nearest neighbor's. Thus, it contains the details of the intermolecular interactions.

The Hirshfeld surface of the molecule mapped over the $d_{norm}$ is shown in Figure 4. Hirshfeld surfaces and two-dimensional fingerprint plots are generated using CrystalExplorer17.5 software [38]. The $d_{norm}$ value is positive for shorter contacts (blue region), negative for longer contacts (red regions) compared to van der Waals (vdW) separation. It is zero (white) for the contacts around the vdW separation. The computed molecular Hirshfeld surface area is 193.86 Å², which encloses the volume of 182.08 Å³. Other calculated shape descriptors are globularity (G = 0.801) and a sphericity (Ω = 0.235). The bright red regions on the Hirshfeld surface are due to O-H···O (a) and C-H···O (b) intermolecular interactions.

The 2D fingerprint plot provides a precise two-dimensional graphical representation of the intermolecular interactions in a crystal. The contributions from different contacts to the total Hirshfeld surface area are O···H (31.5%), H···H (23.4%), C···H (15.8%), and F···H (15.4%). The major contributors are O···H and F···H contacts, which are the short intermolecular interactions. The general contributions of the different contacts to the total Hirshfeld surface area are shown in Figure 5.

The short intermolecular O-H contacts are represented by sharp spikes with $d_i+d_e$ = 2 Å. The wings (see Figure 6c) are due to C-H contacts with $d_i+d_e$ values of 3.2 Å. Here $d_i$ and $d_e$ are the distance from the Hirshfeld surface to the nucleus internal to the surface and the distance from the Hirshfeld surface to the nucleus external to the surface, respectively. The central green color region indicates the C-H···π interactions. The contributions of different contacts such as O-H, H-H, C-H, and F-H to the total surface area and the corresponding $d_{norm}$ surface are shown in Figure 6.

### 3.3. Shape index, curvedness, and electrostatic potential

The shape index and curvedness are the two properties of the Hirshfeld surface. The shape index and curvedness are properties to scale the morphology of the crystal. The shape index is a measure of 'which shape' [39]. The shape index map can be used to identify the complementary pairs (red colored hollows and blue-colored bumps) where two surfaces touch each other. These triangular patterns of hollows and bumps on the shape index surface shed light on close interplanar contacts. Proper triangular patterns are not observed on the shape index map.

Curvedness is a measure of 'how much shape'. The flat regions correspond to low values of curvedness and explicate the characteristic arrangement of planar stacking of the molecules in the crystal [40]. Sharp regions on the plot show the high values of curvedness. The molecule shows flat regions on the curvedness map indicating the planar arrangement.

Electrostatic potential map on the Hirshfeld surface indicates the complementarity between the adjacent molecules. The red and blue colored regions on the electrostatic potential map show the hydrogen bond acceptors and hydrogen bond donors respectively. The red colored regions are present around the oxygen atom showing the hydrogen bond acceptor. Fragment patches on the Hirshfeld surface show the molecular interactions corresponding to their coordination number. Hirshfeld surfaces mapped with shape index, curvedness, electrostatic potential, and fragment patches are shown in Figure 7.

### 3.4. 3D energy frameworks

The energy frame works gives insight about the supramolecular association of the molecules in the crystal. The energy framework calculations were performed using Crystal Explorer17.5 software [38] by employing symmetry operations using the B3LYP/6-31G(d,p) functional basis set.

A cluster of molecules within a radius of 3.8 Å was generated around a molecule. The molecules involved in the calculation of interaction energies along the *c* axis is shown in Figure 8. The electrostatic polarization, dispersion, and repulsion energies between the molecular pairs were calculated and listed in Table 3. The *R* is the distance between the mean atomic positions (molecular centroids). The scaling factors used for benchmarked energies for B3LYP/6-31G(d,p) are $k_{ele}$ = 1.015, $k_{pol}$ = 0.740, $k_{disp}$ = 0.871, and $k_{rep}$ = 0.618 [41].

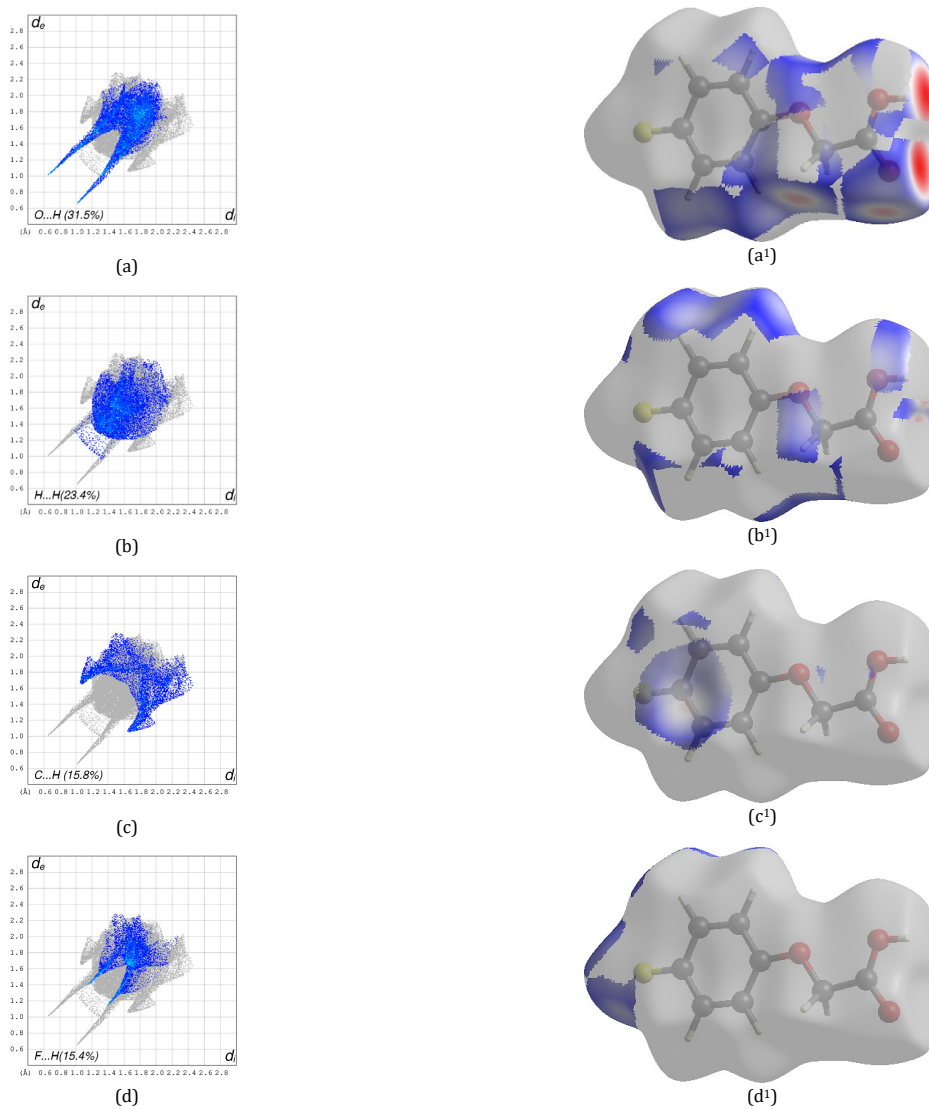(a)

(b)

(c)

(d)

(a¹)

(b¹)

(c¹)

(d¹)

**Figure 6.** The 2D fingerprint plot of the molecule from various contributions. (a), (b), (c), and (d) indicate the interactions from O-H, H-H, C-H, and F-H, respectively. (a¹), (b¹), (c¹), and (d¹) represent the corresponding $d_{norm}$ surfaces, respectively.
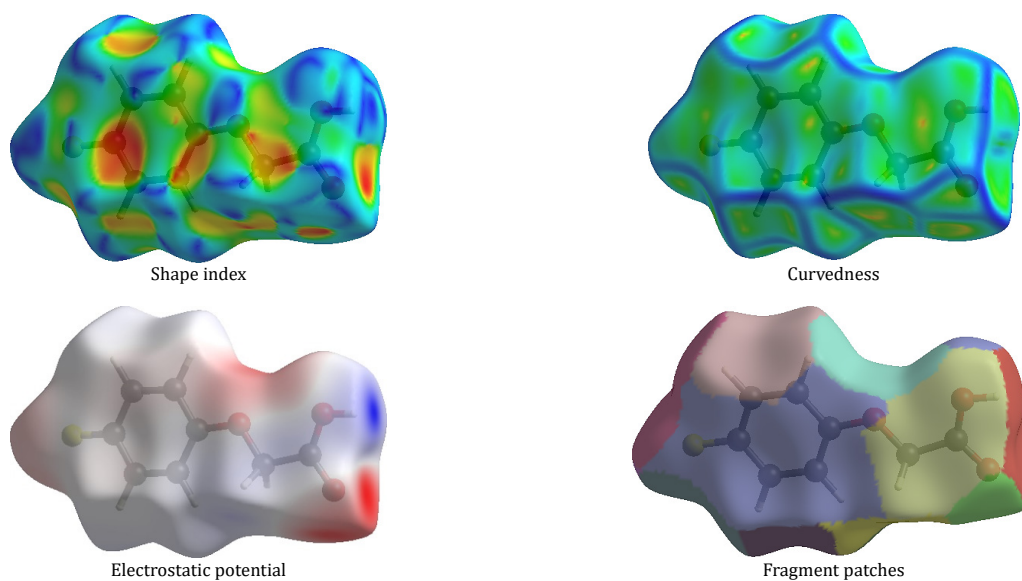


Shape index

Curvedness

Electrostatic potential

Fragment patches

**Figure 7.** Hirshfeld surface mapped with shape index, curvedness, electrostatic potential, and fragment patches.

**Table 3.** Different interaction energies of molecular pairs in kJ/mol.

| Color | N | Symop | R | Electron Density | E_ele | E_pol | E_dis | E_rep | E_tot |
|---|---|---|---|---|---|---|---|---|---|
|  | 1 | *x, y, z* | 4.99 | B3LYP/6-31G(d,p) | -11.2 | -1.9 | -35.4 | 22.5 | -30.3 |
|  | 2 | *x, -y+1/2, z+1/2* | 5.8 | B3LYP/6-31G(d,p) | -4.2 | -0.9 | -13.1 | 6 | -12.8 |
|  | 2 | *x, -y+1/2, z+1/2* | 7.61 | B3LYP/6-31G(d,p) | -2.1 | -0.4 | -8.6 | 4.4 | -7.3 |
|  | 1 | *-x, y+1/2, -z+1/2* | 9.01 | B3LYP/6-31G(d,p) | 0.6 | -0.2 | -3.4 | 0.3 | -2.3 |
|  | 1 | *-x, -y, -z* | 10.04 | B3LYP/6-31G(d,p) | -5.3 | -0.6 | -7 | 5.2 | -8.8 |
|  | 1 | *-x, -y, -z* | 7.59 | B3LYP/6-31G(d,p) | 6.6 | -1.9 | -16.8 | 7.4 | -4.5 |
|  | 1 | *x, y+1/2, -z+1/2* | 6.98 | B3LYP/6-31G(d,p) | -8.3 | -3.1 | -8 | 11.4 | -11 |

**Table 4.** Comparison of bond lengths.

| Atoms | XRD (Å) | DFT (Å) | |
|---|---|---|---|
|  |  | 6-31G(d,p) | 6-31+G(d,p) |
| C2-F1 | 1.363(2) | 1.352 | 1.363 |
| C2-C7 | 1.367(3) | 1.386 | 1.385 |
| C3-C2 | 1.373(3) | 1.393 | 1.392 |
| C3-C4 | 1.385(2) | 1.390 | 1.392 |
| C4-C5 | 1.385(2) | 1.403 | 1.403 |
| C5-C6 | 1.386(2) | 1.399 | 1.399 |
| C6-C7 | 1.388(3) | 1.399 | 1.401 |
| O8-C5 | 1.379(2) | 1.372 | 1.374 |
| O8-C9 | 1.411(2) | 1.410 | 1.409 |
| C9-C10 | 1.496(2) | 1.519 | 1.518 |
| C10-O11 | 1.261(2) | 1.211 | 1.213 |
| C10-O12 | 1.256(2) | 1.344 | 1.344 |

**Table 5.** Comparison of bond angles.

| Atoms | XRD (°) | DFT (°) | |
|---|---|---|---|
|  |  | 6-31G(d,p) | 6-31+G(d,p) |
| C5-O8-C9 | 115.7(1) | 118.3 | 118.1 |
| F1-C2-C7 | 118.7(2) | 119.0 | 118.8 |
| C3-C2-C7 | 122.6(2) | 121.5 | 121.9 |
| F1-C2-C3 | 118.7(2) | 119.1 | 118.8 |
| C2-C3-C4 | 118.3(2) | 119.0 | 118.8 |
| C3-C4-C5 | 120.3(2) | 120.2 | 120.2 |
| O8-C5-C4 | 115.5(1) | 115.3 | 115.4 |
| O8-C5-C6 | 124.4(1) | 124.7 | 124.5 |
| C4-C5-C6 | 120.1(2) | 119.9 | 119.9 |
| C5-C6-C7 | 119.8(2) | 119.7 | 119.8 |
| C2-C7-C6 | 118.9(2) | 119.3 | 119.1 |
| O8-C9-C10 | 111.5(1) | 111.4 | 111.5 |
| O11-C10-C9 | 114.8(1) | 121.7 | 121.6 |
| O12-C10-C9 | 120.7(1) | 114.2 | 114.4 |
| O11-C10-O12 | 124.5(1) | 124.0 | 123.8 |
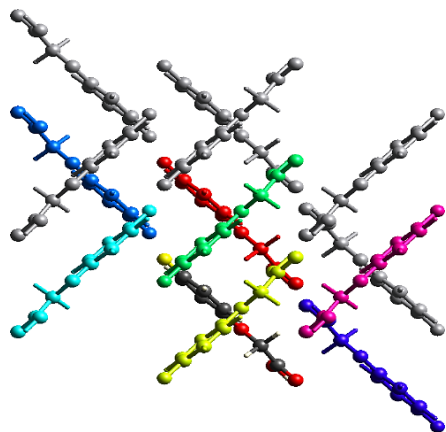


**Figure 8.** Molecules involved in the calculation of the interaction energies along the *c-axis.*

The pictorial representation of Coulomb energy, dispersion energy, and the total interaction energy of the molecule viewed along *a*, *b*, and *c* axis is shown in green, red, and blue colors respectively and are displayed in Figure 9. The different interaction energies viz., electrostatic, dispersion, polarization, and repulsion energies are -163.2, -134.2, -43.5, and 220.3 kJ/mol, respectively. The total energy is -186.1 kJ/mol. The electrostatic energy dominates over the dispersion energy. The lattice energy of the molecule is -69.85 kJ/mol. The cylinders in the energy framework depict the relative strengths of the molecular packing and the associated energies between the molecular pairs in different directions [42]. The absence of cylinders along a particular direction is due to weak interactions below a threshold energy and they are omitted for the less crowded appearance.

### 3.5. Density functional theory

The computational quantum mechanical method was employed to study the electronic structure and chemical properties of the molecule. The quantum computational method, density functional theory (DFT) calculations were carried out using Gamess software [43]. Geometric calculations were performed using B3LYP hybrid functionals with 6-31G(d,p) and 6-31+G(d,p) as basis sets. The geometry optimization and vibrational analysis also were also carried out. The frontier molecular orbitals; Highest Occupied Molecular Orbitals (HOMO) and Lowest Unoccupied Molecular Orbitals (LUMO) were studied to ascertain the chemical stability of the molecule.

The theoretically predicted values of bond length, bond angles, and torsion angles are in good agreement with the experimental values. Comparison of theoretical and experimental values is listed in Tables 4-6. It is inferred that the optimized molecule is not a stationary point on the molecular potential energy surface. Frequency calculations were performed and are tabulated (Table 7). Imaginary frequencies were not observed. The optimized structure of the molecule is shown in Figure 10.

**Table 6.** Comparison of torsion angles in degree.

| Atoms | XRD (°) | DFT (°) | |
|---|---|---|---|
| | | 6-31G(d,p) | 6-31+G(d,p) |
| C9-O8-C5-C4 | −176.1(1) | -178.8 | -178.8 |
| C9-O8-C5-C6 | 4.8(2) | 1.1 | 1.1 |
| C5-O8-C9-C10 | 174.7(1) | 178.5 | 178.5 |
| C3-C2-C7-C6 | −0.4(3) | -0.0 | -0.0 |
| F1-C2-C3-C4 | −179.3(2) | -179.9 | -179.9 |
| F1-C2-C7-C6 | −179.9(2) | -179.9 | -180.0 |
| C7-C2-C3-C4 | 1.2(3) | 0.0 | 0.0 |
| C2-C3-C4-C5 | −0.9(3) | -0.0 | 0.0 |
| C3-C4-C5-C6 | −0.1(2) | -0.0 | -0.0 |
| C3-C4-C5-O8 | −179.3(2) | 179.9 | 179.8 |
| C4-C5-C6-C7 | 0.9(3) | 0.1 | 0.1 |
| O8-C5-C6-C7 | 180.0(2) | -179.9 | -179.9 |
| C5-C6-C7-C2 | −0.6(3) | -0.0 | -0.0 |
| O8-C9-C10-O11 | 180.0(1) | 179.9 | -179.6 |
| O8-C9-C10-O12 | −0.2(2) | -0.1 | 0.3 |

**Table 7.** Interaction energies.

| Parameters | E (kJ/mol) | H (kJ/mol) | G (kJ/mol) | CV (J/mol.K) | CP (J/mol.K) | S (J/mol.K) |
|---|---|---|---|---|---|---|
| Electronic | 0.000 | 0.000 | 0.000 | 0.000 | 0.000 | 0.000 |
| Translational | 3.718 | 6.197 | -45.323 | 12.472 | 20.786 | 172.800 |
| Rotational | 3.718 | 3.718 | -34.873 | 12.472 | 12.472 | 129.436 |
| Vibrational | 424.957 | 424.957 | 313.706 | 172.888 | 172.888 | 373.137 |
| Total | 432.394 | 434.873 | 233.511 | 197.831 | 206.145 | 675.373 |
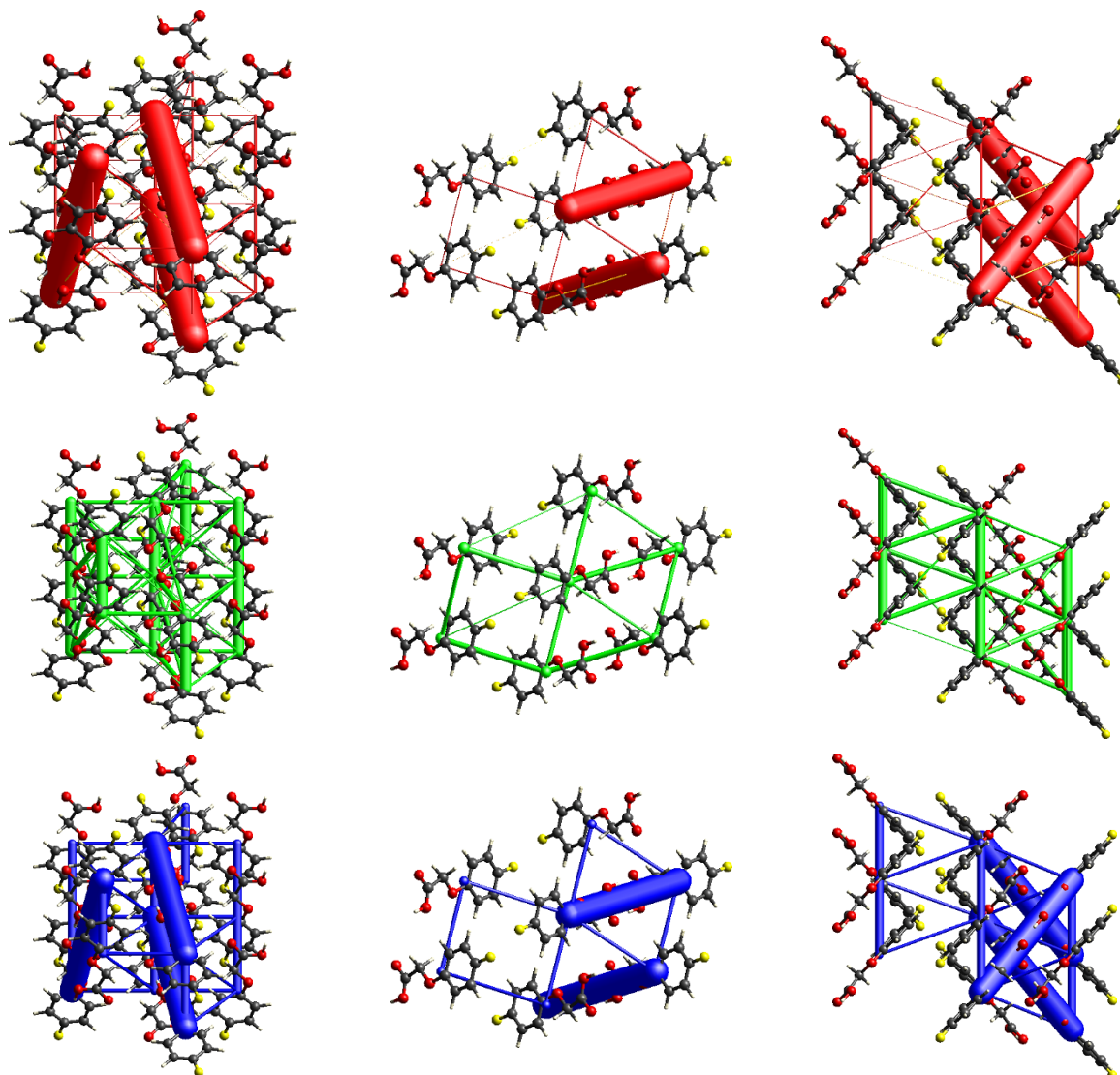


**Figure 9.** Representation of the Coulomb interaction energy, dispersion energy, and total energy in red, green, and blue colors along the *a, b,* and *c* axes, respectively.

**Table 8.** Global reactivity descriptors and their estimated energy values.

| Descriptor | Energy |
|---|---|
| HOMO | -6.41 eV |
| LUMO | -0.89 eV |
| Energy difference (ΔE) | 5.51 eV |
| Ionization potential (I) | 6.41 eV |
| Electron affinity (A) | 0.89 eV |
| Chemical potential (μ) | -3.81 eV |
| Electronegativity (χ) | 3.81 eV |
| Global hardness (η) | 2.76 eV |
| Global softness (σ) | 0.36 eV$^{-1}$ |
| Electrophilicity (ω) | 2.63 eV |
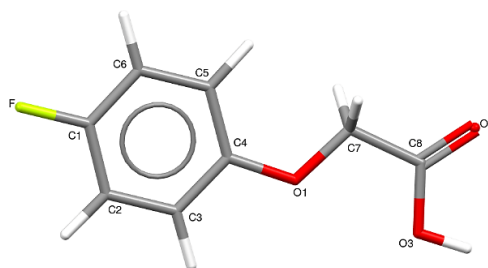


**Figure 10.** The optimized structure of the molecule.
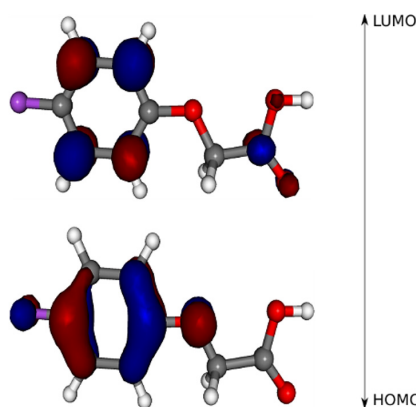


**Figure 11.** HOMO-LUMO energy level of the molecule.

### 3.6. Frontier molecular orbitals

The frontier molecular orbitals viz., HOMO and LUMO and the energy difference between them is computed with the exchange correlation functional B3LYP/6-31+G(d,p) basis set. HOMO acts as an electron donor, and LUMO acts as an electron acceptor. The energy gap between HOMO and LUMO is 5.51 eV. The molecule is highly stable and less reactive compared to other molecules [44]. The energy gap of the molecule predicts the stability and reactivity [45]. HOMO is localized in the phenoxy ring. The energy level of the molecular orbitals HOMO and LUMO of the molecule is shown in Figure 11. To understand the chemical reactivity of the molecule, molecular descriptors have been studied. The molecular descriptors, viz. ionization potential (I), electron affinity (A), chemical potential (μ), electronegativity (χ), global softness (σ), global hardness (η), and electrophilicity (ω) are listed in Table 8. The global parameters were calculated using the formulae, $I = -E_{HOMO}$, $A = E_{LUMO}$, $\chi = 1/2(I + A)$, $\mu = -\chi$, $\eta = \Delta E/2$, $\sigma = 1/\eta$, and $\omega = \mu^2/2\eta$.

### 3.7. Molecular electrostatic potential

The molecular electrostatic potential (MEP) map illustrates the charge distribution of molecules in three dimensions. The values of electrostatic potential determine the electrophilic or nucleophilic reactive sites. The molecular electrostatic potential map is generated by covering all atoms of a molecule at van der Waals radius of the atoms. It is calculated for the regions distributed evenly on the van der Waals surface. The regions obtained are color coded [46]. The red colored regions on the MEP map indicate the negative electrostatic potential (regions of attraction for positive charge). The blue colored regions indicate the positive electrostatic potential (regions of attraction for negative charge). The intermediate potential values are indicated by yellow, green, and light blue colored regions. The distribution of electrostatic potential on the molecular surface is shown in Figure 12. It shows that the negative electrostatic potential is spread over the oxygen atom and the positive electrostatic potential is concentrated around the hydrogen atom attached to the phenoxy ring.
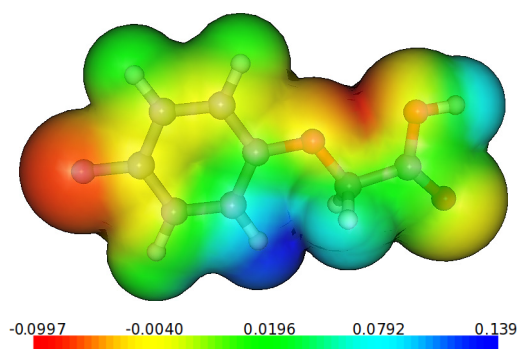


**Figure 12.** Molecular electrostatic potential map of the molecule.

## 4. Conclusions

The molecule, 2-(4-fluorophenoxy) acetic acid, crystallizes in the monoclinic crystal system with the space group $P2_1/c$. Hirshfeld surface analysis revealed the C-H···O intermolecular interactions in the crystal. The three-dimensional energy frameworks indicate that the electrostatic energy is dominant over the dispersion energy. DFT calculations were carried over B3LYP/6-31+G(d,p) basis set infers that the theoretically predicted structural values are in good agreement between the experimental values. The energy gap between HOMO and LUMO is 5.51 eV, which implies the stability of the molecule. The analysis of the molecular electrostatic potential surface revealed the electronegative and electropositive sites are around the oxygen and hydrogen atoms, respectively.

## Acknowledgement

## Supporting information Ⓢ

CCDC-1949545 contains the supplementary crystallo-graphic data for this paper. These data can be obtained free of charge via https://www.ccdc.cam.ac.uk/structures/ or by e-mailing data_request@ccdc.cam.ac.uk or by contacting The Cambridge Crystallographic Data Centre, 12 Union Road, Cambridge CB2 1EZ, UK; fax: +44(0)1223-336033.

## Disclosure statement Ⓓ

Conflict of interests: The authors declare that they have no conflict of interest.
Author contributions: All authors contributed equally to this work.
Ethical approval: All ethical guidelines have been adhered.
Sample availability: Samples of the compounds are available from the author.

## ORCID Ⓘ

Akhileshwari Prabhuswamy
Ⓘ https://orcid.org/0000-0003-0716-3542
Yasser Hussein Eissa Mohammed
Ⓘ https://orcid.org/0000-0003-1086-7292
Fares Hezam Al-Ostoot
Ⓘ https://orcid.org/0000-0003-4571-6419
Geetha Doddanahalli Venkatesh
Ⓘ https://orcid.org/0000-0001-8628-8794
Sridhar Mandayam Anandalwar
Ⓘ https://orcid.org/0000-0002-3065-3630
Shaukath Ara Khanum
Ⓘ https://orcid.org/0000-0003-1713-4489
Lokanath Neratur Krishnappagowda
Ⓘ https://orcid.org/0000-0003-2773-2247

## References

[1]. Geetha, D. V.; Al-Ostoot, F. H.; Mohammed, Y. H. E.; Sridhar, M. A.; Khanum, S. A.; Lokanath, N. K. *J. Mol. Struct.* **2019**, *1178*, 384–393.

[2]. Sharma, G.; Anthal, S.; Geetha, D. V.; Al-Ostoot, F. H.; Hussein Eissa Mohammed, Y.; Ara Khanum, S.; Sridhar, M. A.; Kant, R. *Mol. Cryst. Liq. Cryst.* **2018**, *675* (1), 85–95.

[3]. Mohammed, Y. H. E.; Malojirao, V. H.; Thirusangu, P.; Al-Ghorbani, M.; Prabhakar, B. T.; Khanum, S. A. *Eur. J. Med. Chem.* **2018**, *143*, 1826–1839.

[4]. Haupt, K.; Dzgoev, A.; Mosbach, K. *Anal. Chem.* **1998**, *70* (3), 628–631.

[5]. Zhang, H.; Song, T.; Zong, F.; Chen, T.; Pan, C. *Int. J. Mol. Sci.* **2008**, *9* (1), 98–106.

[6]. Mokale, S. N.; Nevase, M. C.; Sakle, N. S.; Dube, P. N.; Shelke, V. R.; Bhavale, S. A.; Begum, A. *Bioorg. Med. Chem. Lett.* **2014**, *24* (9), 2155–2158.

[7]. Begum, S.; Bharathi, K.; Prasad, K. *Int. J. Pharm. Pharm. Sci.* **2016**, *8* (10), 66–71.

[8]. Wang, X.; Zhao, T.; Yang, B.; Li, Z.; Cui, J.; Dai, Y.; Qiu, Q.; Qiang, H.; Huang, W.; Qian, H. *Bioorg. Med. Chem.* **2015**, *23* (1), 132–140.

[9]. Kumara, K.; Al-Ostoot, F. H.; Mohammed, Y. H. E.; Khanum, S. A.; Lokanath, N. K. *Chem. Data Coll.* **2019**, *20* (100195), 100195.

[10]. Takeda, Y.; Kawagoe, K.; Yokomizo, A.; Yokomizo, Y.; Hosokami, T.; Ogihara, Y.; Honda, Y.; Yokohama, S. *Chem. Pharm. Bull. (Tokyo)* **1998**, *46* (3), 434–444.

[11]. Dahiya, R.; Kaur, R. *Aust. J. Basic App. Sci.* **2007**, *1* (4), 525-532. http://www.ajbasweb.com/old/ajbas/525-532.pdf (accessed Jul 31, 2021).

[12]. Shahar Yar, M.; Bakht, M. A.; Siddiqui, A. A.; Abdullah, M. M.; De Clercq, E. *J. Enzyme Inhib. Med. Chem.* **2009**, *24* (3), 876–882.

[13]. Chandrika, P. M.; Yakaiah, T.; Rao, A. R. R.; Narsaiah, B.; Reddy, N. C.; Sridhar, V.; Rao, J. V. *Eur. J. Med. Chem.* **2008**, *43* (4), 846–852.

[14]. Rani, P.; Pal, D., Kumar; Hegde, R., Rama; Hashim, S., Riaz. *Hem. Ind.* **2015**, *69* (4), 405–415.

[15]. Tipparaju, S. K.; Muench, S. P.; Mui, E. J.; Ruzheinikov, S. N.; Lu, J. Z.; Hutson, S. L.; Kirisits, M. J.; Prigge, S. T.; Roberts, C. W.; Henriquez, F. L.; Kozikowski, A. P.; Rice, D. W.; McLeod, R. L. *J. Med. Chem.* **2010**, *53* (17), 6287–6300.

[16]. Sun, A.; Prussia, A.; Zhan, W.; Murray, E. E.; Doyle, J.; Cheng, L.-T.; Yoon, J.-J.; Radchenko, E. V.; Palyulin, V. A.; Compans, R. W.; Liotta, D. C.; Plemper, R. K.; Snyder, J. P. *J. Med. Chem.* **2006**, *49* (17), 5080–5092.

[17]. Nikalje, A. P. G.; Deshpande, D.; Une, H. D. *Euro. J. Exp. Bio.* **2012**, *2* (2), 343-353. https://www.imedpub.com/articles/facile-synthesis-and-iin-vivoi-hypoglycemic-activity-of-novel-2-4hiazolidinedione-derivatives.pdf (accessed Jul 31, 2021).

[18]. Al-Ostoot, F. H.; Geetha, D. V.; Mohammed, Y. H. E.; Akhileshwari, P.; Sridhar, M. A.; Khanum, S. A. *J. Mol. Struct.* **2020**, *1202* (127244), 127244.

[19]. Al-Ostoot, F. H.; Mohammed, Y. H. E.; Zabiulla, A. N. K.; Khanum, S. A. *J. Appl. Pharm. Sci.* **2019**, *9* (7), 42–49.

[20]. Eissa Mohammed, Y. H.; Thirusangu, P.; Vigneshwaran, V.; Prabhakar, B. T.; Khanum, S. A. *Biomed. Pharmacother.* **2017**, *95*, 375–386.

[21]. Northover, B. J.; Verghese, J. *J. Pharm. Pharmacol.* **1962**, *14* (1), 615–616.

[22]. Harsanyi, S.; Zamborsky, R.; Krajciova, L.; Kokavec, M.; Danisovic, L. *Medicina (Kaunas)* **2020**, *56* (4), 153.

[23]. Yang, X.; Xu, P.; Gao, Q.; Tan, M. *Synth. React. Inorg. Met.-Org. Nano-Met. Chem.* **2002**, *32* (1), 59–68.

[24]. Sun, Z.; Ding, B.; Wu, B.; You, Y.; Ding, X.; Hou, X. *J. Phys. Chem. C Nanomater. Interfaces* **2012**, *116* (3), 2543–2547.

[25]. Thomas, M. G.; Lawson, C.; Allanson, N. M.; Leslie, B. W.; Bottomley, J. R.; McBride, A.; Olusanya, O. A. *Bioorg. Med. Chem. Lett.* **2003**, *13* (3), 423–426.

[26]. Ramadan, E. M.; Abou-Taleb, K. A.; Galal, G. F.; Abdel-Hamid, N. S. *Ann. Agric. Sci.* **2017**, *62* (2), 151–159.

[27]. Al-Ostoot, F. H.; Stondus, J.; Anthal, S.; Venkatesh, G. D.; Mohammed, Y. H. E.; Sridhar, M. A.; Khanum, S. A.; Kant, R. *Eur. J. Chem.* **2019**, *10* (3), 234–238.

[28]. Khamees, H. A.; Mohammed, Y. H. E.; Ananda; Al-Ostoot, F. H.; Sangappa; Alghamdi, S.; Khanum, S. A.; Madegowda, M. *J. Mol. Struct.* **2020**, *1199* (127024), 127024.

[29]. Khamees, H. A.; Mohammed, Y. H. E.; Swamynayaka, A.; Al-Ostoot, F. H.; Sert, Y.; Alghamdi, S.; Khanum, S. A.; Madegowda, M. *ChemistrySelect* **2019**, *4* (15), 4544–4558.

[30]. Smith, G.; Lynch, D. E.; Sagatys, D. S; Kennard, C. H. L.; Katekar, G. F. *Aust. J. Chem.* **1992**, *45* (7), 1101–1108.

[31]. Mohammed, Y. H. I.; Naveen, S.; Mamatha, S. V.; Jyothi, M.; Khanum, S. A.; Lokanath, N. K. *IUCrdata* **2016**, *1* (10), x161714. https://doi.org/10.1107/s2414314616017144.

[32]. Ahmad, N. A.; Naveen, S.; Karthik Kumara, K.; Jamalis, J.; Lokanath, N. K. *Der Pharma Chem.* **2016**, *8* (2), 49–53.

[33]. Rigaku, CrystalClear, Rigaku Corporation, Tokyo, Japan, 2011.

[34]. Sheldrick, G. M. *Acta Crystallogr. A* **2008**, *64* (Pt 1), 112–122.

[35]. Spek, A. L. *Acta Crystallogr. D Biol. Crystallogr.* **2009**, *65* (Pt 2), 148–155.

[36]. Macrae, C. F.; Sovago, I.; Cottrell, S. J.; Galek, P. T. A.; McCabe, P.; Pidcock, E.; Platings, M.; Shields, G. P.; Stevens, J. S.; Towler, M.; Wood, P. A. *J. Appl. Crystallogr.* **2020**, *53* (Pt 1), 226–235.

[37]. McKinnon, J. J.; Spackman, M. A.; Mitchell, A. S. *Acta Crystallogr. B* **2004**, *60* (Pt 6), 627–668.

[38]. Mackenzie, C. F.; Spackman, P. R.; Jayatilaka, D.; Spackman, M. A. *IUCrJ* **2017**, *4* (Pt 5), 575–587.

[39]. Spackman, M. A.; Jayatilaka, D. *CrystEngComm* **2009**, *11* (1), 19–32.

[40]. McKinnon, J. J.; Jayatilaka, D.; Spackman, M. A. *Chem. Commun. (Camb.)* **2007**, No. 37, 3814–3816.

[41]. Turner, M. J.; Grabowsky, S.; Jayatilaka, D.; Spackman, M. A. *J. Phys. Chem. Lett.* **2014**, *5* (24), 4249–4255.

[42]. Turner, M. J.; Thomas, S. P.; Shi, M. W.; Jayatilaka, D.; Spackman, M. A. *Chem. Commun. (Camb.)* **2015**, *51* (18), 3735–3738.

[43]. Schmidt, M. W.; Baldridge, K. K.; Boatz, J. A.; Elbert, S. T.; Gordon, M. S.; Jensen, J. H.; Koseki, S.; Matsunaga, N.; Nguyen, K. A.; Su, S.; Windus, T. L.; Dupuis, M.; Montgomery, J. A. *J. Comput. Chem.* **1993**, *14* (11), 1347–1363.

[44]. Akhileshwari, P.; Kiran, K. R.; Sridhar, M. A.; Sadashiva, M. P.; Lokanath, N. K. *J. Mol. Struct.* **2021**, *1242* (130747), 130747.

[45]. Bendjeddou, A.; Abbaz, T.; Ayari, A.; Benahmed, M.; Gouasmia, A.; Villemin, D. *Orient. J. Chem.* **2016**, *32* (2), 799–806.

[46]. Gasteiger, J.; Li, X.; Rudolph, C.; Sadowski, J.; Zupan, J. *J. Am. Chem. Soc.* **1994**, *116* (11), 4608–4620.